


Optical detection of paramagnetic defects in diamond grown by chemical vapor depositionC. Pellet-Mary¹, P. Huillery¹, M. Perdriat¹, A. Tallaire², and G. Hétet¹¹*Laboratoire de Physique de l'Ecole Normale Supérieure, ENS, Université PSL, CNRS, Sorbonne Université, Université Paris-Diderot, Sorbonne Paris Cité, 75005 Paris, France*²*IRCP, Ecole Nationale Supérieure de Chimie de Paris, 11 rue Pierre et Marie Curie, 75005 Paris, France* (Received 5 December 2020; revised 10 March 2021; accepted 10 March 2021; published 24 March 2021)

The electronic spins of the nitrogen-vacancy (NV) centers in chemical-vapor-deposition (CVD) grown diamonds form ideal probes of magnetic fields and temperature, as well as promising qubits for quantum information processing. Studying and controlling the magnetic environment of NV centers in such high-purity crystals is thus essential for these applications. We demonstrate optical detection of paramagnetic species, such as hydrogen-related complexes, in a CVD-grown diamond. The resonant transfer of the NV centers' polarized electronic spins to the electronic spins of these species generates conspicuous features in the NV photoluminescence when employing magnetic field scans along the [100] crystal direction. Our results offer prospects for more detailed studies of CVD-grown processes as well as for coherent control of the spin of novel classes of hyperpolarized paramagnetic species.

DOI: [10.1103/PhysRevB.103.L100411](https://doi.org/10.1103/PhysRevB.103.L100411)

The electronic spin properties of the negatively charged nitrogen-vacancy (NV⁻) center in diamond have given rise to a wealth of applications in nanoscale sensing [1] and quantum information science [2]. One major reason is that NV⁻ can be optically polarized and read out and features long coherence time even at ambient conditions. In order to optimize the capabilities of the NV center, its magnetic environment must be very well controlled. Synthetic growth of diamond crystals is now reaching a level of maturity that makes the most pristine diamond crystals almost flawless, thus eliminating the source of magnetic noise from nearby impurities other than the NV sensor. The standard growth technique works through chemical vapor deposition (CVD) of carbon atoms from a methane gas in an ultrahigh-vacuum environment. It offers the possibility to use crystals with 99.9% purity, as well as using ¹²C enriched methane, hence removing spin fluctuations from ¹³C atoms and enhancing further the sensing capabilities of NV centers [3].

Electron paramagnetic resonance (EPR) spectroscopy is the method of choice for controlling the concentration of paramagnetic defects in materials. Thanks to their high resolution, EPR spectrometers are also essential tools for understanding the conformation of many defects that remain in CVD-grown diamond materials [4–6]. However, compared to confocal microscopy, this equipment is rather bulky and less cost-effective. It would also be ideal if these defects were detected with the very same technology that is employed for nanoscale sensing [1] and quantum information processing [7]. This technology would, indeed, offer the opportunity to hyperpolarize these defects using the optically polarized NV center and to employ them as quantum bits at ambient conditions.

Here, we use confocal laser microscopy to detect paramagnetic defects via the coupling to a high-density NV

spin ensemble in a CVD-grown diamond. Figure 1 shows a schematic of the various paramagnetic defects that have been coupled to the nitrogen-vacancy center and detected optically in our study. These are the negatively charged vacancy-hydrogen center (VH⁻) and WAR1 defects, two spin-1 defects with zero-field splitting comparable to that of the NV⁻ center [5,8], as well as ¹³C spin 1/2 nuclear spins, through hyperfine coupling with a secondary NV⁻ center. The detection is realized by measuring the NV photoluminescence while performing magnetic field scans to resonantly enhance dipole-dipole interactions and observe cross relaxations (CRs). Cross relaxation typically takes place when the electronic or nuclear spins of two atomic species exchange their polarizations via resonant magnetic dipole-dipole interactions. If the spin of NV center A is polarized and coupled to unpolarized spin B with a much larger relaxation rate, it will lose part of its polarization at the expense of B and thus see a drop in its photoluminescence (PL) rate. Tuning the frequency of both spin transitions so that they are coresonant will result in a reduction of the PL of NV A, thus enabling detection of the spin energy of B.

The negatively charged nitrogen-vacancy center has a zero-field splitting $D = (2\pi)2.87$ GHz in the ground state, related to the dipole-dipole interaction between the spin of the two unpaired electrons. One of the most important properties of the spin of the NV⁻ center is that it can be optically polarized and read out and features long relaxation time (approximately milliseconds) even at ambient conditions, which can be used to detect other species via CR and even to polarize them. Many paramagnetic defects in diamond also carry a spin of 1. Their zero-field splittings are, in fact, their fingerprint. To measure them, one can tune the angle and magnitude of an external magnetic field angle to cause cross relaxation with the NV centers. The obtained CR position can

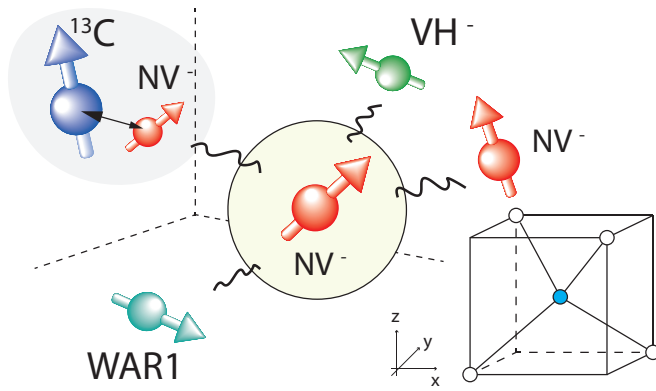


FIG. 1. Schematics showing various paramagnetic defects in CVD-grown diamonds interacting with the electronic spin of a negatively charged nitrogen-vacancy center. Inset: Atomic positions in the diamond unit cell.

then be used to trace back the zero-field splittings of the defects.

Previous cross-relaxation studies with NV^- centers were mostly carried out using heavily doped crystals grown by the high-pressure, high-temperature (HPHT) process [9–14]. Recent efforts in doping processes have also made it possible to reach NV^- center concentrations in the 3 to 5 ppm range in CVD-grown samples [15–17], opening a path towards detecting other paramagnetic defects in CVD-grown diamonds. The sample we use is the pink irradiated sample presented in [16]. It was grown using CVD with the addition of 500 ppm of N_2O to the H_2/CH_4 (96/4) gas phase. Then high-energy (10 MeV) electron irradiation at a fluence of $2 \times 18 \text{ cm}^{-2}$ and at a temperature of 900°C was realized, giving a final concentration of NV^- of about 4.6 ppm. The initial concentration of nitrogen in the sample was about 25 ppm. It was shown that T_2^* was not degraded after annealing, yet the NV^- density was large enough to enable concentration-dependent longitudinal relaxation [16,18].

In this study, we use a homebuilt confocal microscope that comprises a 1-mW green laser and an objective with a numerical aperture of 0.25 to focus the laser onto the sample as well as to collect the NV^- photoluminescence. The PL was filtered from the green laser using a dichroic mirror and a notch filter. It was then coupled to a multimode fiber and detected by an avalanche photodiode. The magnetic field scans were realized using a C-shaped electromagnet driven by a current generator (HP 33120A). We then monitored the NV^- PL synchronously with the changes in the magnetic field. Contrary to the more commonly employed [111] direction, we scan the magnetic field along the diamond [100] crystalline direction. Looking at the diamond structure (bottom right in Fig. 1), it can be noticed that, in this direction, the projections of NV^- centers (or any other C_{3v} defect) along the magnetic field are identical, which means the transition energies of the different classes of NV^- centers cannot cross under a B field scan along this direction. This method could otherwise result in several low-field PL features under arbitrary angles [19,20] that could mask cross relaxation from other species and also reduce the CR contrast (see Sec. 4 of the Supplementary Material [21] (SM) for data showing scans along the [111]

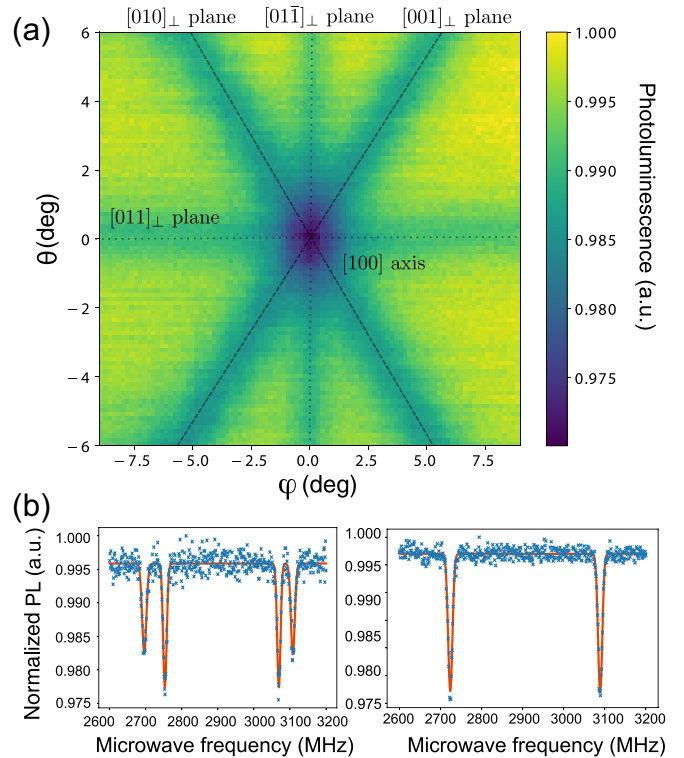


FIG. 2. (a) NV^- photoluminescence as a function of the magnetic field angle around the [100] crystalline direction at a fixed amplitude $|\vec{B}| = 115 \text{ G}$. The planes orthogonal to the [010], [001], [011], and $[01\bar{1}]$ directions are indicated by dashed lines. (b) Left: Optically detected magnetic resonance (ODMR) spectrum taken at the angular position $(\phi, \theta) = (3^\circ, 3^\circ)$. Right: ODMR spectrum taken at the exact center of the map, i.e., the [100] direction.

direction). The downside of this choice of the [100] direction is that at large amplitudes, the transverse component of the magnetic field depolarizes all classes of NV^- s, thus limiting the magnetic field range that can be employed and restricting this detection method to paramagnetic defects with zero-field splittings close to the NV^- center's.

In order to identify the [100] direction, we perform an angular scan of the magnetic field using a dual-axis goniometer (Thorlabs GNL20-Z8) that holds a permanent magnet at a fixed distance from the sample. Figure 2(a) shows the NV^- photoluminescence as a function of magnetic field direction, referenced by azimuthal and polar angles (ϕ, θ) with respect to the [100] direction, using the above-described CVD-grown sample. The PL is seen to drop for particular values of the magnet angular coordinates that correspond to specific crystalline axes. Such a drop in the PL, also observed in [18–20,22–25], correspond to transitions of NV^- centers becoming degenerate. The planes orthogonal to the [010], [001], [011], and $[01\bar{1}]$ directions are indicated by dashed lines and show the locus of the cross relaxation. They all cross on the [100] axis. The origin of these sharp changes in the photoluminescence was attributed to cross relaxation between polarized NV^- centers and rapidly decaying NV^- centers, so-called fluctuators [25]; the precise origin of the latter remains unknown. The width of the CR features when the magnetic field crosses a plane perpendicularly was found to be compatible with the

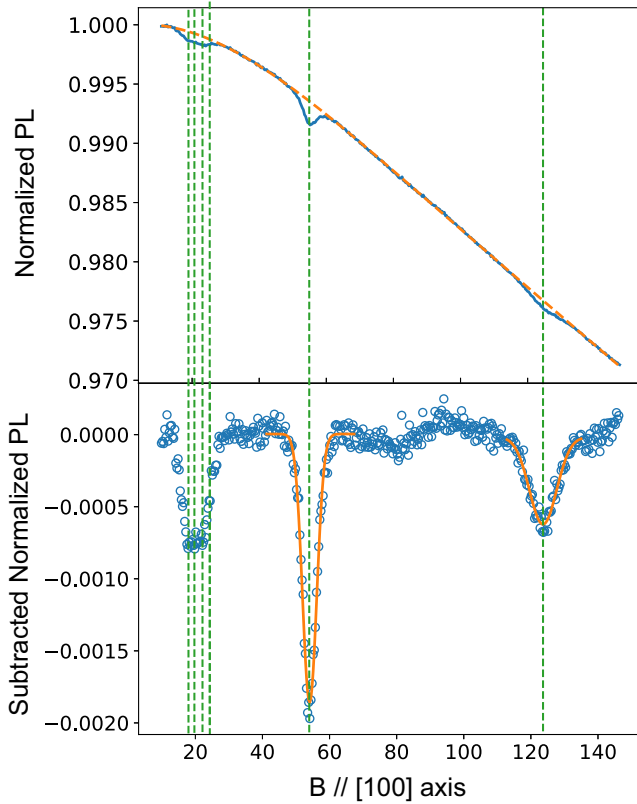


FIG. 3. Optical detection of cross relaxations. Top: NV^- photoluminescence counts as a function of the magnetic field amplitude along the [100] crystalline direction (solid line) and fourth-order polynomial fit (dashed line). Bottom: Curve obtained by subtracting the polynomial fit to the above signal (circles). The simulated cross-relaxation positions are shown by the green dashed vertical lines. Gaussian fits to the second and third dips are shown by solid orange lines.

NV^- decoherence rate (≈ 6 MHz). The contrast is determined both by the fluctuating NV^- and polarized NV^- concentrations.

Such a map can, in itself, be useful for measuring magnetic fields without microwaves [20]. It also enables us to identify the crystalline axes. To verify that the central line is the [100] axis, we realize microwave scans around the NV^- transitions. Away from the crystal planes, we consistently observe eight optically detected magnetic resonance (ODMR) lines coming from the four $|m_s = 0\rangle$ to $|m_s = \pm 1\rangle$ spin transitions of the $\{111\}$ -oriented NV^- centers. On the planes orthogonal to the [010], [001], [011], and $[0\bar{1}1]$ directions, however, we expect degeneracies. Figure 2(b) shows an ODMR spectrum taken at $(\phi, \theta) = (3^\circ, 3^\circ)$. As expected, at this position, two pairs of NV^- classes cross. Figure 2(b) shows an electron spin resonance taken at the angle $(\phi, \theta) = (0^\circ, 0^\circ)$ showing only two features, as expected for a [100] axis. Using this goniometer, the magnetic field angle could be finely adjusted so that the NV^- lines become fully degenerate along the [100] direction with an error estimate of $\pm 0.5^\circ$.

Figure 3 shows the PL as a function of magnetic field amplitude along the [100] direction, in the 15- to 145-G range. Calibration of the magnetic field amplitude was realized by applying microwave signals at varying frequencies in 2-MHz

TABLE I. Zero-field splitting parameter D for the spin-1 species in our sample.

	D_z estimation (MHz)	
	Cruddace's work [8]	Our work
NV^-	2872(7)	
VH^-	2706(30)	2694(5)
WAR1	2466(60)	2470(10)

steps on several magnetic field scans. The microwave-induced PL features in the scan are then used to relate the magnetic field to the applied voltage. Three features appear in this spectrum at 20, 56, and 122 G. Data averaging was done for 24 h, but the features appear already with a signal-to-noise ratio greater than 1 after 10 min. We also observe an overall drop in the PL as a result of state mixing in the optically excited state [2]. To let the three salient features detach better from the spectrum, we fitted a fourth-order polynomial to the broad PL change, without the spectral bumps, and subtracted it from the data. Further details on the fitting choices are provided in Sec. 5 of the SM [21].

In order to attribute the three features to their respective defects, we run a similar scan (Sec. 1 in the SM [21]) on a type Ib electron-irradiated HPHT diamond crystal with a NV^- concentration in the 5–20-ppm range. Only the first feature appeared. This observation guided us to search for CVD-related defects as candidates for the last two features. Paramagnetic defects in CVD-grown diamonds have been extensively studied using EPR [26]. These studies demonstrate that hydrogen-related complexes such as nitrogen-vacancy-hydrogen center, VH^- , VH_2 can be stable in diamond. Although their compositions is not always known, several zero-field splittings D can be found in the literature. Given the small difference between the NV^- transitions and the observed features, we concentrate on only reported defects with zero-field splitting (ZFS) that are close to the NV^- . The second column of Table I shows the zero-field splitting for two such spin-1 defects found in [8], namely, the negatively charged hydrogen vacancy (VH^-) and WAR1 defects. The latter was analyzed in EPR, but its exact structure is unknown [8]. Figure 4 shows the frequencies of the NV^- , VH^- , and WAR1 spin transitions as a function of the magnetic field amplitude along the [100] direction. Since NV^- and VH^- are C_{3v} defects and WAR1 is a pseudo- C_{3v} defect [8], all possible orientations are degenerate at this magnetic field orientation, giving only two lines corresponding to the $|0\rangle \rightarrow |+1\rangle$ and $|0\rangle \rightarrow |-1\rangle$ transitions. The points where the NV^- levels cross the other defects can give rise to cross relaxation.

Using this theoretical calculation, we find that the second peak in Fig. 3 coincides very well with a CR that would occur at the crossing between the $|m_s = 0\rangle$ to $|m_s = -1\rangle$ NV^- transition and the $|m_s = 0\rangle$ to $|m_s = +1\rangle$ VH^- transition. A Gaussian fit to the feature in Fig. 3 enables us to extrapolate a value of $D = 2694(5)$ MHz that matches that of the VH^- within the error margins indicated in [8]. The third peak at 122 G corresponds to a spin defect that has $D = 2470(10)$ MHz that also matches that of the WAR1 defect. The values of D for these two defects and the error bars from our measurements are included in Table I. The error bars are estimated by taking

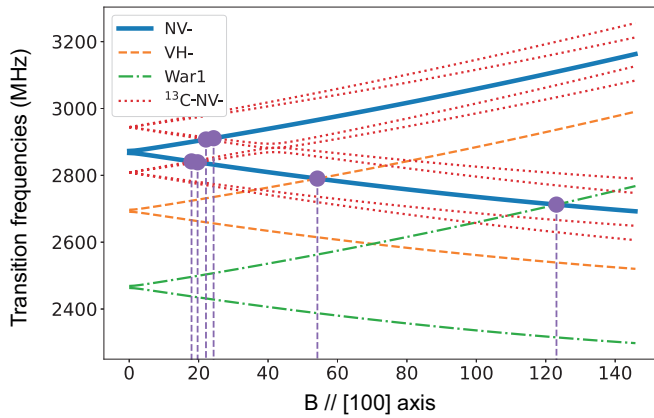


FIG. 4. Simulated transition energies of the various considered spins as a function of a magnetic field aligned to the [100] axis. The NV centers' electronic spin transitions are shown by the thick solid line, VH^- are shown using dashed lines, WAR1 are shown using dash-dotted lines, and the ^{13}C -NV pair is shown using dotted lines. The amplitudes of the magnetic field where the energy level of the NV center crosses that of another species are represented by vertical dashed lines.

into account the precision on the NV^- ZFS, on the angle, and on the magnetic field calibration and the precision of the fits. We obtain a factor of 6 improvement over the precision reported in [8] and attribute the second and third features to cross relaxation between the NV center and the VH^- and WAR1 defects. Scans along the [111] direction shown in the SM [21] also corroborate this conclusion.

The remaining broader feature in the spectrum could be coming from dipolar coupling between the spin of NV centers and paramagnetic defects that are present also in HPHT-grown diamonds, such as the substitutional nitrogen, also called P_1 centers ($[P_1] \approx 5\text{--}20$ ppm in our sample) or the ^{13}C atoms (natural isotopic abundance [^{13}C] = 1%). Using the results from [27], we first intended to correlate its spectral position to the transitions of dipolar-coupled NV and P_1 centers. P_1 centers have a zero-field splitting of only 100 MHz. In order to cross one of the two NV spin transitions at a magnetic field of 20 G, they would then have to be coupled off resonantly to the spin of nearby NV centers. The resulting pair could then be coupled resonantly to a nearby polarized NV. The obtained eigenfrequencies of the dipolar coupled P_1 -NV pair that we extracted were all inconsistent with the spectral positions of our observed peak within our spectral resolution error (≈ 1 G) (see Sec. 3 of the SM [21]). This leads us to consider instead the nuclear spin of the ^{13}C atoms as the most likely candidate.

The nuclear spin of the ^{13}C atoms does not have a ZFS, and its gyromagnetic factor is four orders of magnitude lower than that of the electron. Here again, in order to give a CR contribution to the spectrum at modest magnetic fields, the nuclear spin of ^{13}C would first have to be strongly coupled to an NV center. The resulting pair could then be coresonant with the spin transitions of a bare NV center, as depicted in Fig. 1. This situation can manifest itself when the nuclear spin of ^{13}C atoms is a few shells away from the nitrogen-vacancy centers. A strong hyperfine coupling rate of 130 MHz can, for instance, be reached with a ^{13}C that is only one shell away from the NV center. In contrast, higher-order shells have a maximum hyperfine coupling of 15 MHz [28], making them hard to distinguish from the inhomogeneous broadening. The modeling of this interaction is presented in Sec. 2 of the SM [21]. The dotted lines in Fig. 4 show the four transition frequencies of the first-shell ^{13}C coupled to an NV center. The crossings between the $|m_s = 0\rangle$ to $|m_s = \pm 1\rangle$ NV transition and the four transitions of this ^{13}C -NV pair occur at magnetic field values around 20 G. We added these four lines to the experimental spectrum shown in Fig. 3. Good agreement is found between the magnetic field at which of these four transitions cross the NV and the broad 20-G feature, letting us conclude that it is the result of a CR between an unpolarized ^{13}C -NV pair and a polarized NV center.

Because the sample we use has a very well determined concentration of ^{13}C (natural 1.1% abundance), we can use the first CR peak to calibrate the concentration of VH^- and WAR1 in our sample. There are three possible sites for a first-shell ^{13}C -NV pair, so the concentration of ^{13}C -NV pairs is about 3.3% that of the NV centers, i.e., ~ 135 ppb. Comparing the area of the second and third peaks to that of the first one, we find $[VH^-] \approx 195$ ppb and $[WAR1] \approx 124$ ppb. Using areas is more relevant here than using amplitudes because inhomogeneous spread overwhelms the spin-spin interaction. Note that the WAR1 concentration is probably underestimated due to state mixing in the NV centers at the NV-WAR1 magnetic field for CR.

In conclusion, we demonstrated all-optical detection of paramagnetic species in a diamond grown by the chemical-vapor-deposition method. We identified three-body interactions between the spin of NV centers and ^{13}C -NV pairs as well as cross relaxations between NV centers and the VH^- and WAR1 defects. Our results offer prospects for more detailed studies of CVD-grown processes as well as for realizing quantum networks with these newly coupled spins.

We would like to thank N. Manson and C. Meriles for fruitful discussions and L. Mayer for lending us a highly doped test sample. The authors would also like to thank SIRTEQ for funding. G.H. also acknowledges funding from the French National Research Agency (ANR) through the T-ERC project QUOVADIS.

[1] L. Rondin, J.-P. Tetienne, T. Hingant, J.-F. Roch, P. Maletinsky, and V. Jacques, *Rep. Prog. Phys.* **77**, 056503 (2014).

[2] M. W. Doherty, N. B. Manson, P. Delaney, F. Jelezko, J. Wrachtrup, and L. C. Hollenberg, *Phys. Rep.* **528**, 1 (2013).

- [3] J. Achard, V. Jacques, and A. Tallaire, *J. Phys. D* **53**, 313001 (2020).
- [4] M. E. Newton, *ChemInform* **38**, 131 (2007).
- [5] C. Glover, M. E. Newton, P. M. Martineau, S. Quinn, and D. J. Twitchen, *Phys. Rev. Lett.* **92**, 135502 (2004).
- [6] C. Glover, M. E. Newton, P. Martineau, D. J. Twitchen, and J. M. Baker, *Phys. Rev. Lett.* **90**, 185507 (2003).
- [7] N. Y. Yao, L. Jiang, A. V. Gorshkov, P. C. Maurer, G. Giedke, J. I. Cirac, and M. D. Lukin, *Nat. Commun.* **3**, 800 (2012).
- [8] R. Cruddace, Ph.D. thesis, University of Warwick, 2007.
- [9] R. J. Epstein, F. M. Mendoza, Y. K. Kato, and D. D. Awschalom, *Nat. Phys.* **1**, 94 (2005).
- [10] H.-J. Wang, C. S. Shin, S. J. Seltzer, C. E. Avalos, A. Pines, and V. S. Bajaj, *Nat. Commun.* **5**, 4135 (2014).
- [11] S. Armstrong, L. J. Rogers, R. L. McMurtrie, and N. B. Manson, *Phys. Procedia* **3**, 1569 (2010).
- [12] L. T. Hall, P. Kehayias, D. A. Simpson, A. Jarmola, A. Stacey, D. Budker, and L. C. L. Hollenberg, *Nat. Commun.* **7**, 10211 (2016).
- [13] A. Wickenbrock, H. Zheng, L. Bougas, N. Leefer, S. Afach, A. Jarmola, V. M. Acosta, and D. Budker, *Appl. Phys. Lett.* **109**, 053505 (2016).
- [14] N. Alfasi, S. Masis, O. Shtempluck, and E. Buks, *Phys. Rev. B* **99**, 214111 (2019).
- [15] A. M. Edmonds, C. A. Hart, M. J. Turner, P.-O. Colard, J. M. Schloss, K. Olsson, R. Trubko, M. L. Markham, A. Rathmill, B. Horne-Smith, W. Lew, A. Manickam, S. Bruce, P. G. Kaup, J. C. Russo, M. J. DiMario, J. T. South, J. T. Hansen, D. J. Twitchen, and R. L. Walsworth, [arXiv:2004.01746](https://arxiv.org/abs/2004.01746).
- [16] A. Tallaire, O. Brinza, P. Huillery, T. Delord, C. Pellet-Mary, R. Staacke, B. Abel, S. Pezzagna, J. Meijer, N. Touati, L. Binet, A. Ferrier, P. Goldner, G. Hetet, and J. Achard, *Carbon* **170**, 421 (2020).
- [17] Y. Mindarava, R. Blinder, C. Laube, W. Knolle, B. Abel, C. Jentgens, J. Isoya, J. Scheuer, J. Lang, I. Schwartz, B. Naydenov, and F. Jelezko, *Carbon* **170**, 182 (2020).
- [18] A. Jarmola, A. Berzins, J. Smits, K. Smits, J. Prikulis, F. Gahbauer, R. Ferber, D. Erts, M. Auzinsh, and D. Budker, *Appl. Phys. Lett.* **107**, 242403 (2015).
- [19] E. van Oort and M. Glasbeek, *Appl. Magn. Reson.* **2**, 291 (1991).
- [20] R. Akhmedzhanov, L. Gushchin, N. Nizov, V. Nizov, D. Sobgayda, I. Zelensky, and P. Hemmer, *Phys. Rev. A* **100**, 043844 (2019).
- [21] See Supplemental Material at <http://link.aps.org/supplemental/10.1103/PhysRevB.103.L100411> for further experimental and simulation details, which includes Refs. [27,29–32].
- [22] E. van Oort and M. Glasbeek, *Phys. Rev. B* **40**, 6509 (1989).
- [23] R. Akhmedzhanov, L. Gushchin, N. Nizov, V. Nizov, D. Sobgayda, I. Zelensky, and P. Hemmer, *Phys. Rev. A* **96**, 013806 (2017).
- [24] K. Holliday, N. B. Manson, M. Glasbeek, and E. v. Oort, *J. Phys.: Condens. Matter* **1**, 7093 (1989).
- [25] J. Choi, S. Choi, G. Kucsko, P. C. Maurer, B. J. Shields, H. Sumiya, S. Onoda, J. Isoya, E. Demler, F. Jelezko, N. Y. Yao, and M. D. Lukin, *Phys. Rev. Lett.* **118**, 093601 (2017).
- [26] M. N. R. Ashfold, J. P. Goss, B. L. Green, P. W. May, M. E. Newton, and C. V. Peaker, *Chem. Rev.* **120**, 5745 (2020).
- [27] M. Simanovskaia, K. Jensen, A. Jarmola, K. Aulenbacher, N. Manson, and D. Budker, *Phys. Rev. B* **87**, 224106 (2013).
- [28] B. Smeltzer, L. Childress, and A. Gali, *New J. Phys.* **13**, 025021 (2011).
- [29] G. A. Álvarez, C. O. Bretschneider, R. Fischer, P. London, H. Kanda, S. Onoda, J. Isoya, D. Gershoni, and L. Frydman, *Nat. Commun.* **6**, 8456 (2015).
- [30] F.-J. Jiang, J.-F. Ye, Z. Jiao, Z.-Y. Huang, and H.-J. Lv, *Chin. Phys. B* **27**, 057601 (2018).
- [31] E. J. Kamp, B. Carvajal, and N. Samarth, *Phys. Rev. B* **97**, 045204 (2018).
- [32] R. Lazda, L. Busaite, A. Berzins, J. Smits, F. Gahbauer, M. Auzinsh, D. Budker, and R. Ferber, [arXiv:2007.00473](https://arxiv.org/abs/2007.00473) [Phys. Rev. B (to be published)].